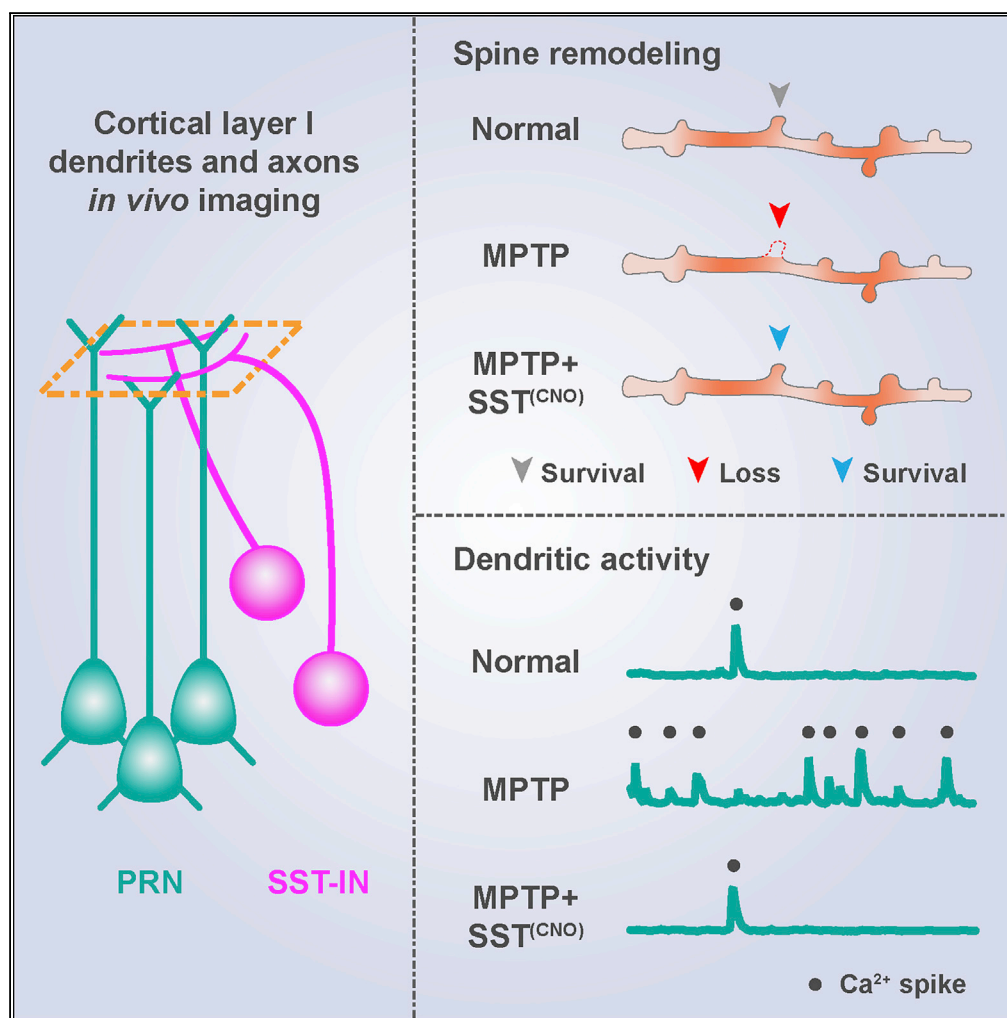**Article**

Activation of Cortical Somatostatin Interneurons Rescues Synapse Loss and Motor Deficits after Acute MPTP Infusion

Kai Chen, Guang Yang, Kwok-Fai So, Li Zhang

gy2268@cumc.columbia.edu (G.Y.)
hrmaskf@hku.hk (K.-F.S.)
zhangli@jnu.edu.cn (L.Z.)

HIGHLIGHTS

Acute MPTP infusion induces cortical spine loss and motor learning deficits

MPTP hyperactivates dendritic Ca^{2+} spikes and suppresses SST-interneuron activity

Chemogenetics activation of SST-interneuron corrects spine loss and motor deficits

Article

Activation of Cortical Somatostatin Interneurons Rescues Synapse Loss and Motor Deficits after Acute MPTP Infusion

Kai Chen,[1] Guang Yang,[2,*] Kwok-Fai So,[1,3,4,5,6,*] and Li Zhang[1,5,6,7,*]

SUMMARY

Adult dendritic spines present structural and functional plasticity, which forms the basis of learning and memory. To provide *in vivo* evidence of spine plasticity under neurotoxicity, we generated an acute motor deficit model by single injection of 1-methyl-4-phenyl-1,2,3,6-tetrahydropyridine (MPTP) into adult mice. Acute MPTP infusion impairs motor learnings across test paradigms. *In vivo* two-photon imaging further revealed MPTP-induced prominent dendritic spine loss and substantially increased calcium spikes in apical tufts of layer 5 pyramidal neurons in the motor cortex. MPTP infusion also decreased the activity of somatostatin (SST)-expressing inhibitory interneurons. Further chemogenetic re-activation of SST interneurons reversed MPTP-induced hyperactivation of dendrites, rescued spine loss, and enhanced motor learning. Taken together, our study reports MPTP-induced structural and functional deficits of dendritic spines and suggests the potency of modulating local inhibitory transmission to relieve neurological disorders.

INTRODUCTION

The learning of new motor skills leads to the genesis of postsynaptic dendritic spines in the motor cortex, and the retention of motor memory is associated with the maintenance of these learning-related new spines (Cichon and Gan, 2015; Xu et al., 2009, 2012; Yang et al., 2009, 2014). Under pathological conditions such as those in Parkinson disease (PD), dendritic spines in the motor cortex present instability and high levels of turnover (Guo et al., 2015). Agreeing with these findings, functional magnetic resonance imaging studies reveal pathological hyperactivity in the motor cortex of patients with PD (Pelled et al., 2002; Sabatini et al., 2000; Yu et al., 2007). Such evidence suggests dysfunctions of the motor cortex in motor learning impairments (Guo et al., 2015; Sabatini et al., 2000). Therefore, further studies for the relationship among synaptic activity, spine activity, and motor function may provide implications for the intervention of motor disorders.

Many lines of evidence indicate that the generation and propagation of Ca^{2+} spikes in pyramidal neuron dendrites coordinate synaptic activity and facilitate synaptic potentiation and/or depotentiation (Cichon and Gan, 2015; Weber et al., 2016). Dendritic Ca^{2+} spikes participate in the strengthening and/or remodeling of dendritic spines during both development and motor learning (Li et al., 2017), whereas aberrant dendritic activity is associated with synaptic depotentiation in the diseased brain (Bai et al., 2017). The generation of Ca^{2+} spikes is heavily regulated by local inhibitory interneurons, which also play an important role in modulating structural synaptic changes in pyramidal cells (Hattori et al., 2017). In Alzheimer disease (AD), dysfunction of somatostatin-expressing inhibitory interneurons (SST-INs) results in progressive hippocampal synapse loss (Schmid et al., 2016). Following repeated stress in mice, decreased activity of parvalbumin-expressing inhibitory interneurons causes a high rate of dendritic spine elimination in the somatosensory cortex (Chen et al., 2018). In the motor cortex, a recent study showed that SST-INs are tightly correlated with learning-induced activities of pyramidal neurons (Adler et al., 2019). However, no study has investigated the involvement of SST-INs under pathological conditions.

In this study, we generated an acute motor deficit model by introducing a single dose of 1-methyl-4-phenyl-1,2,3,6-tetrahydropyridine (MPTP), which led to impaired motor memory retention. *In vivo* imaging of the motor cortex revealed enhanced elimination of learning-related dendritic spines, increased pyramidal neuron dendritic activity, as well as decreased activities of SST-INs. Activation of SST-INs in the motor cortex restored dendritic Ca^{2+} activity and synaptic stability and improved motor skill retention. Our results suggest that targeting SST-INs may help to relieve MPTP-induced cortical dysfunction and motor deficits.

[1]Joint International Research Laboratory of CNS Regeneration, Guangdong-Hong Kong-Macau Institute of CNS Regeneration, Jinan University, Guangzhou 510632, China

[2]Department of Anesthesiology, Columbia University Medical Center, New York, NY, USA

[3]State Key Laboratory of Brain and Cognitive Science, Li Ka Shing Faculty of Medicine, The University of Hong Kong, Hong Kong SAR, P. R. China

[4]Co-Innovation Center of Neuroregeneration, Nantong University, Nantong 226019, P. R. China

[5]Guangzhou Regenerative Medicine and Health Guangdong Laboratory, Guangzhou 510530, P. R. China

[6]Center for Brain Science and Brain-Inspired Intelligence, Guangdong-Hong Kong-Macao Greater Bay Area, Guangzhou 510515, P. R. China

[7]Lead Contact

*Correspondence: gy2268@cumc.columbia.edu (G.Y.), hrmaskf@hku.hk (K.-F.S.), zhangli@jnu.edu.cn (L.Z.)

https://doi.org/10.1016/j.isci.2019.06.040

RESULTS

Dendritic Spine Instability and Motor Memory Deficits Induced by Single MPTP Infusion

We repeatedly imaged fluorescently labeled dendritic spines of layer 5 pyramidal neurons (L5PRNs) in the primary motor cortex using transcranial two-photon microscopy (Figure 1A). Results showed that a single intraperitoneal (i.p.) injection of MPTP (30 mg/kg) caused a 2-fold increase in dendritic spine turnover within 4–24 h in 1-month-old mice (MPTP versus vehicle, all in %, 4 h, 9.0 $\pm$ 0.54 versus 4.4 $\pm$ 0.58; 24 h, 18.2 $\pm$ 0.95 versus 10.4 $\pm$ 0.74; p < 0.05 by t test in both cases; Figures 1B and 1C). The rates of spine formation and elimination were both higher in MPTP-treated mice than those in vehicle-treated control mice (MPTP versus vehicle, all in %, elimination: 4 h, 4.2 $\pm$ 0.36 versus 2.5 $\pm$ 0.40; 24 h, 8.0 $\pm$ 0.63 versus 4.2 $\pm$ 0.36; formation: 4 h, 5.3 $\pm$ 0.40 versus 1.9 $\pm$ 0.27; 24 h, 10.2 $\pm$ 0.57 versus 4.8 $\pm$ 0.39; p < 0.05 by t test in all comparison pairs). These results indicate that MPTP has potent effects on dendritic spine dynamics in the cortex.

Previous studies have shown that motor learning induces the rapid formation of new spines in the motor cortex, and the persistence of these new spines associated with motor learning is critical for motor memory retention (Yang et al., 2009). We next investigated whether MPTP similarly altered the dynamics of motor learning-induced new spines (Figure 1D). We trained 1-month-old mice to run on an accelerating rotarod or perform a beam walking task, and immediately after motor skill learning, mice were treated with MPTP. Consistent with previous studies (Li et al., 2017; Xu et al., 2009; Yang et al., 2009, 2014), new spine formation increased significantly within 8 h after motor training when compared with untrained controls (all in %, non-learning, 4.4 $\pm$ 0.5; beam learning, 6.2 $\pm$ 0.3; rotarod learning, 6.8 $\pm$ 0.4; p < 0.01 by t test for both comparison pairs; Figures 1E and 1F). We found that among new spines formed within 8 h after motor training, fewer spines persisted over next 4 h (8–12) or 16 h (8–24) in the MPTP-treated mice when compared with vehicle-treated controls (p < 0.01 by t test for both rotarod and beam walking, Figures 1G–1I). Furthermore, motor performance improvement was lower in MPTP-treated mice 1 day or 4 days after motor training (p < 0.05 by t test for both 1 day and 4 days, Figures 1J and 1K). There was a significant correlation between the percentages of motor training-related persistent new spines and motor skill performance improvement (Pearson correlation, rotarod learning, r = 0.78; p = 0.0016; beam learning, r = 0.69; p = 0.0058; Figures 1L and 1M). Together, these results demonstrate dendritic spine instability and impaired motor memory retention by single MPTP administration.

Increased Ca^{2+} Spike Generation in Apical Tuft Dendrites of Pyramidal Neurons

Previous studies have correlated dendritic spine dynamics with the dendritic activity of pyramidal neurons (Cichon and Gan, 2015; Weber et al., 2016). To study cortical activity in MPTP-treated mice, we performed *in vivo* Ca^{2+} imaging in apical tuft branches of L5PRNs (Figure 2C). Wild-type (WT) mice were given intra-cranial injection of an adeno-associated virus (AAV) delivered vector encoding the Ca^{2+} indicator GCaMP6s to monitor pyramidal neuron activity (Figure S1). First, the levels of Ca^{2+} activity in dendritic spines exhibited a 3-fold increase in MPTP-treated mice when compared with vehicle treatment (p < 0.0001 by t test, Figures 2A and 2B). In addition to Ca^{2+} activity in spines, we also observed a substantial increase in dendritic Ca^{2+} spikes following systemic MPTP injection: the number of Ca^{2+} spikes in the field of view (FOV) rapidly increased within 1 h post-injection, reached the peak level at 2 h, and remained higher than the pre-injection baseline at 4 h (p < 0.0001 by two-way ANOVA; Figure 2D). Vehicle treatment had no effects on the generation of dendritic Ca^{2+} spikes (Figures S2A and S2B). Analyses of individual dendrites showed significantly higher Ca^{2+} frequency and integrated Ca^{2+} levels 2 h after MPTP injection relative to pre-injection (p < 0.0001 by two-way ANOVA; Figures 2E–2H, Video S1). The amplitudes of dendritic Ca^{2+} spikes were comparable before and after MPTP injection (Figure S2C). These MPTP-induced dendritic Ca^{2+} spikes were largely reduced in the presence of locally delivered *N*-methyl-D-aspartate (NMDA) receptor antagonist MK801 (p < 0.0001 by t test; Figures 2I and 2J). These results show that MPTP injection causes an increase of dendritic spine and branch activity in pyramidal neuron tufts.

To further understand the effects of MPTP on the cortex, we topically applied MPTP (30 μM in artifical cerebrospinal fluid, aCSF) to the superficial layer of the motor cortex and performed *in vivo* Ca^{2+} imaging on apical dendrites of L5PRNs (Figure 3A). We found that the number of Ca^{2+} spikes in the FOV increased markedly over 30 min after MPTP local application and returned to the baseline 2 h post-washout (150 min post-MPTP) (p < 0.05 by t test, Figures 3B–3D, Video S2). Both frequency and integrated activity of dendritic Ca^{2+} spikes peaked at 30 min after MPTP application and recovered to pre-injection levels 2 h post-washout (p < 0.0001 by two-way ANOVA, Figures 3E and 3F). The amplitudes of dendritic
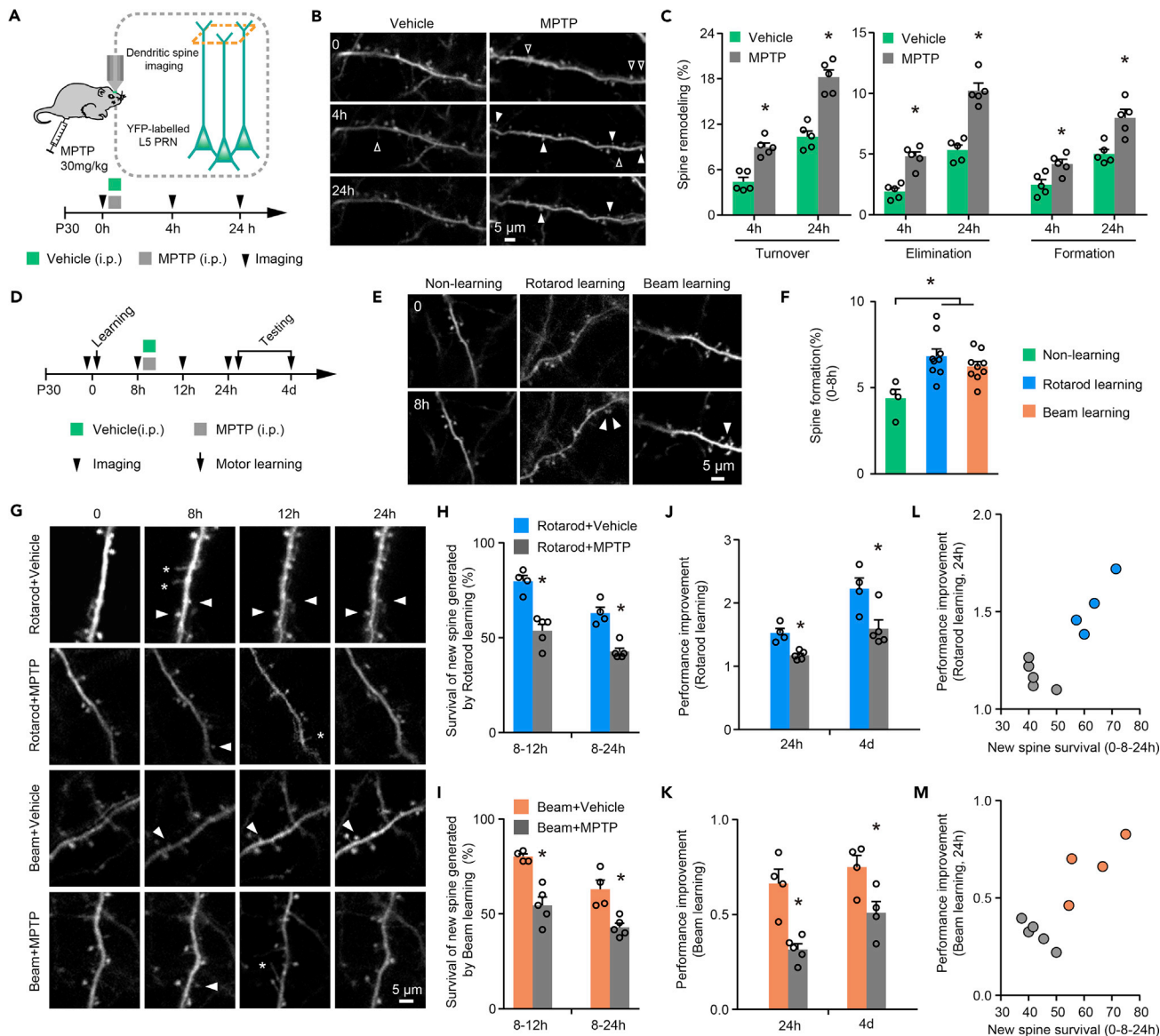
Figure 1. Systemic Administration of MPTP Destabilizes Dendritic Spines and Impairs Motor Memory

(A) Upper, schematic diagram of *in vivo* two-photon imaging in apical dendrites of layer 5 pyramidal neurons (L5PRNs) in the motor cortex of *Thy1*-YFP mice. Lower, timeline of imaging and drug administration.

(B) Representative two-photon images of the same dendritic segment in time series from vehicle or MPTP-treated groups. Filled arrowheads, newly formed spines; open arrowheads, eliminated spines.

(C) From left to right, overall spine turnover, elimination, and formation rates during 0–4 h and 0–24 h. MPTP group showed significantly higher spine plasticity (two-sample student t test; 0–4 h and 0–24 h; turnover, $t_8 = 5.82$, $t_8 = 6.51$; elimination, $t_8 = 6.02$, $t_8 = 6.99$; formation, $t_8 = 3.15$, $t_8 = 4.07$; $p < 0.05$ in all cases. $n = 5$ per group).

(D) Experimental timeline of motor learning and two-photon microscopy.

(E) Representative images of dendritic segments before (0) and after motor learning (8 h).

(F) Spine formation rates over 0–8 h was significantly higher under learning paradigms (non-learning, $n = 4$; beam learning, $n = 9$; rotarod learning, $n = 9$; $F_{(2, 19)} = 7.231$, $p = 0.0046$).

(G–I) (G) Representative dendritic segments in time series before and after motor learning under various conditions. Filled arrowheads, newly formed spine at 8 h; asterisks, filopodia. (H and I) The survival rates of newly formed spines 12 and 24 h after (H) rotarod learning (8–12 h, $t_7 = 5.496$, $p = 0.0009$; 8–24 h, $t_7 = 5.941$, $p = 0.0006$; $n = 4$ in rotarod + vehicle and $n = 5$ in rotarod + MPTP group) or (I) or beam walking learning (8–12 h, $t_7 = 5.130$, $p = 0.0014$; 8–24 h, $t_7 = 4.050$, $p = 0.0049$; $n = 4$ in beam + vehicle and $n = 5$ in beam + MPTP group).

(J and K) Motor performance improvement 24 h and 4 days after (J) rotarod (24 h, $t_7 = 4.867$, $p = 0.0018$; 4 days, $t_7 = 2.916$, $p = 0.0225$) or (K) beam walking learning (24 h, $t_7 = 4.463$, $p = 0.0024$; 4 days, $t_6 = 2.699$, $p = 0.0356$).

(L and M) Pearson correlation analysis showed that new spine survival rates (0–8–24 h) were positively correlated with performance improvement at 24 h in rotarod ($r = 0.78$, $p = 0.0016$; L) and beam walking ($r = 0.69$, $p = 0.0058$; M) assays. *$p < 0.05$. Data were presented as mean ± SEM. Scale bar, 5 μm.
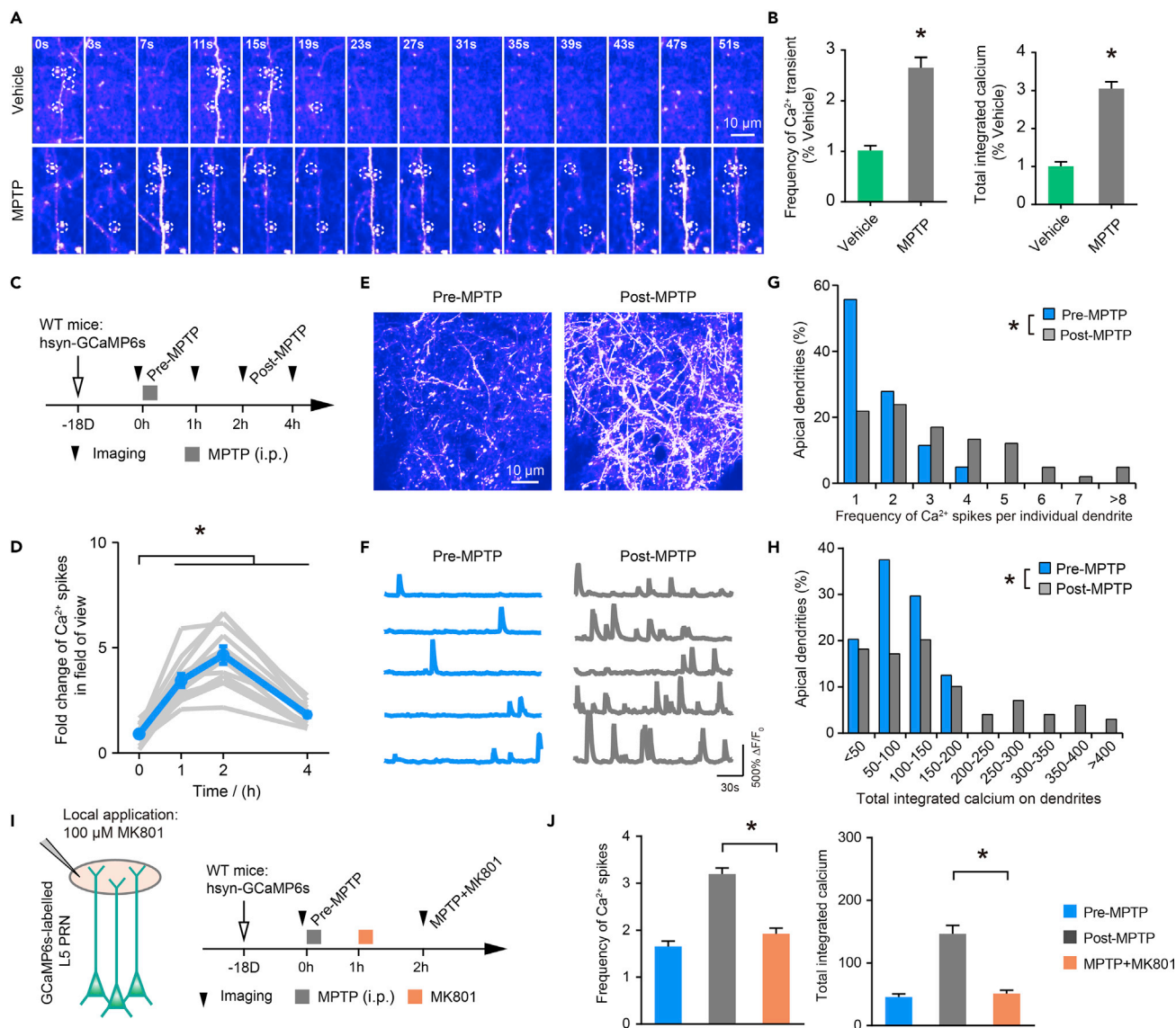
Figure 2. Systemic Administration of MPTP Increases Ca^{2+} Activity in Apical Dendrites of L5PRNs

(A) Representative fluorescence images of dendritic spines in apical tufts of L5PRN expressing GCaMP6s over 50-s time series. Dotted circles, region of interest (ROI) showing Ca^{2+} transients in spines.

(B) MPTP injection significantly increased frequency (t_{98} = 9.30, p < 0.0001) and total integrated levels (t_{98} = 7.32, p < 0.0001) of Ca^{2+} transients in dendritic spines. Vehicle, n = 50 ROIs from four animals; MPTP, n = 50 ROIs from four animals.

(C) Experimental design for apical dendritic imaging after MPTP.

(D) The number of Ca^{2+} spikes in the same field of view (FOV) over hours after MPTP systemic administration (one-way ANOVA, $F_{(3, 44)}$ = 10.18, p < 0.0001; n = 12 FOVs from five mice). Gray, individual traces; blue, averaged levels.

(E) Time-series and z-stacked images showing dendritic Ca^{2+} spikes within 50 s from the same FOV before (pre-MPTP) or 2 h after drug infusion (post-MPTP).

(F) Representative fluorescence traces of L5PRN apical tufts expressing GCaMP6s.

(G) Distribution of Ca^{2+} spike frequency from individual dendritic segments during 3-min sampling windows. MPTP injection significantly increased Ca^{2+} frequency (t_{305} = 3.15, p < 0.0001; n = 61 ROIs before MPTP and n = 246 ROIs post-MPTP from five animals).

(H) Total integrated dendritic Ca^{2+} levels were enhanced by MPTP application (t_{305} = 4.74, p < 0.0001).

(I) Schematic showing MK801 local injection and dendritic Ca^{2+} recording in MPTP-treated mice.

(J) Local application of MK801 reduced dendritic Ca^{2+} spike frequency and averaged dendritic Ca^{2+} activity after MPTP systemic injection (n = 88, t_{332} = 5.54, p < 0.0001).

*p < 0.05. Data were presented as mean ± SEM. Scale bar, 10 μm. See also Figures S1 and S2.
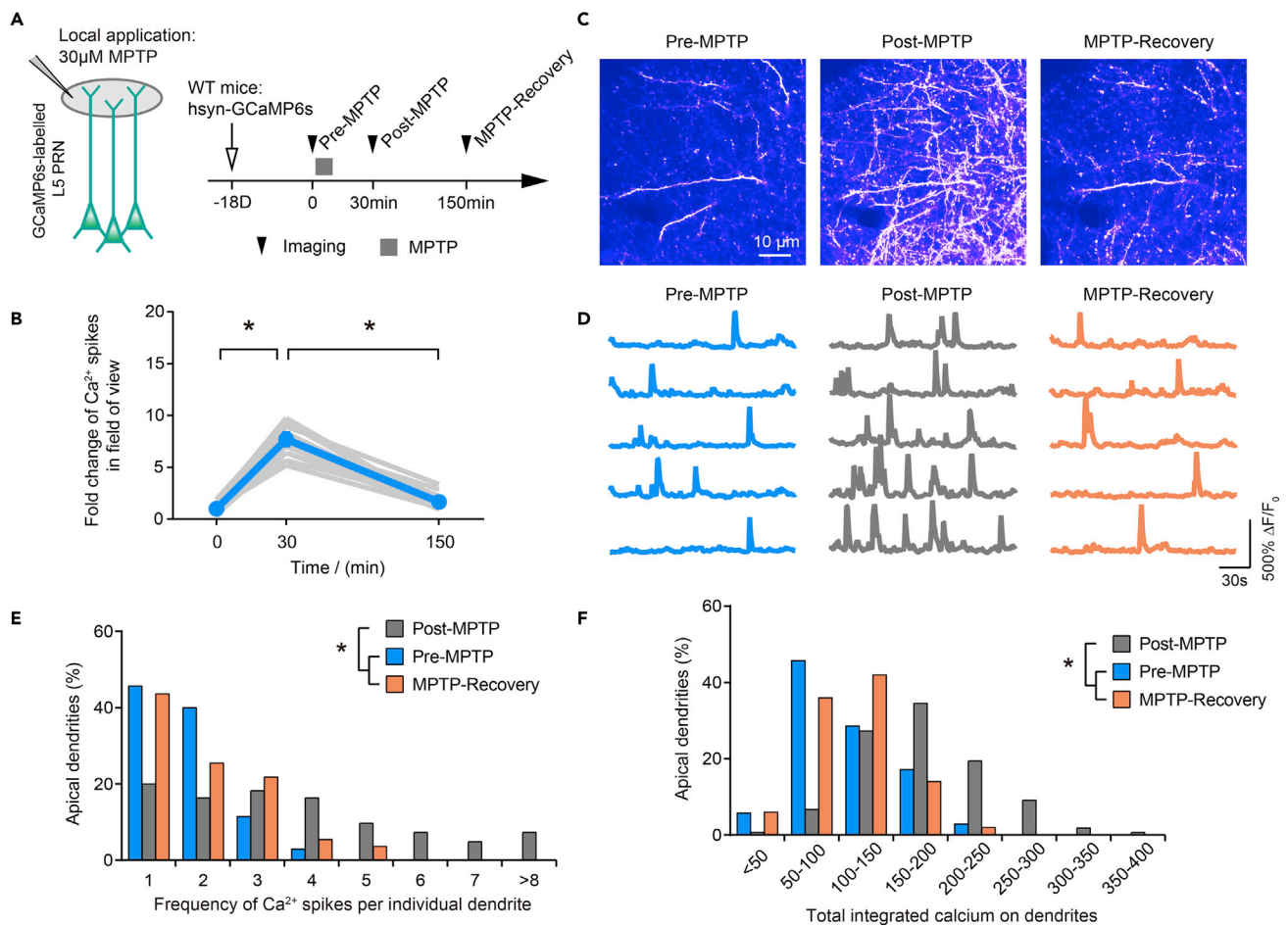
Figure 3. Local Application of MPTP Increases Dendritic Ca²⁺ Activity

(A) Experimental diagram and timeline of MPTP local application and two-photon imaging in L5PRN apical dendrites.

(B) The frequency of dendritic Ca²⁺ spikes rapidly increased after local application of MPTP and returned to baseline levels 150 min later ($F_{(2, 33)}$ = 160.4, $p < 0.0001$; n = 12 fields of view [FOVs] from four mice). Gray, individual traces; blue, averaged levels.

(C) Time-series and z-stacked images showing dendritic Ca²⁺ spikes within 50 s from the same FOV before (pre-MPTP), 30 min after (post-MPTP), and 2 h after removal of drugs (MPTP-recovery). Scale bar, 10 μm.

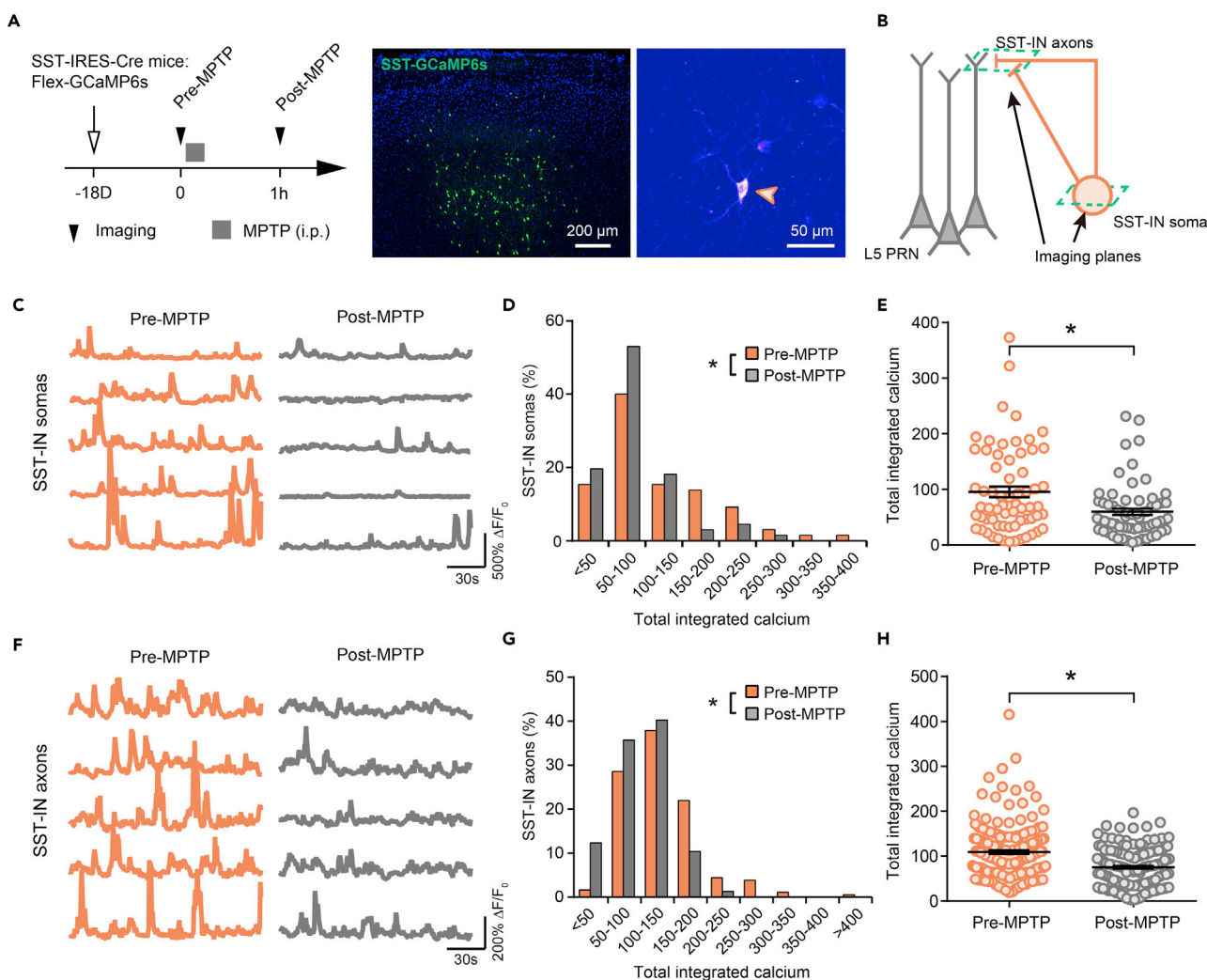(D) Representative fluorescence traces of L5PRN apical dendrites expressing GCaMP6s.

(E) Distribution of dendritic Ca²⁺ spike frequency in individual dendrites over 3-min recording showed significantly elevated Ca²⁺ activity after local MPTP infusion ($F_{(2, 247)}$ = 23.51; $p < 0.0001$; n = 35, 165, and 50 regions of interest from pre-MPTP, post-MPTP, and MPTP-recovery groups, respectively, from four animals).

(F) MPTP application reversibly increased dendritic Ca²⁺ activity averaged over 3-min recording ($F_{(2, 247)}$ = 47.38, $p < 0.0001$) *$p < 0.05$. Data were presented as mean ± SEM.

Ca²⁺ spikes induced by local MPTP are similar to those that occurred after systemic MPTP injection (Figure 2). These results suggest that MPTP-induced dendritic Ca²⁺ spikes are partly mediated by its local action on the cerebral cortex.

Decreased Activity in Somatostatin-Expressing Inhibitory Interneurons

To understand the mechanisms underlying MPTP-induced dendritic activity in pyramidal neurons, we examined the activity of local inhibitory interneurons, focusing on dendritic-targeting SST-INs. These cells project their axons to the superficial layers of the cortex, where they primarily target pyramidal neuron dendrites and form inhibitory synapses (Urban-Ciecko and Barth, 2016). To determine the effects of MPTP on SST-IN activity, we used *in vivo* Ca²⁺ imaging to examine the activity of SST-INs expressing GCaMP6s. Here, SST-*IRES*-Cre mice were injected with a Cre-dependent AAV-dio-GCaMP6s into the motor cortex to induce the expression of GCaMP6s specifically in SST-INs (Figures 4A and 4B). In contrast to the increased activity of dendritic spines and branches in L5PRNs (Figure 2), we found that

Figure 4. MPTP Decreases SST-IN Activity in the Motor Cortex

(A) Left, experimental timeline; middle, expression of GCaMP6s in the motor cortex; right, *in vivo* Ca^{2+} imaging of SST-INs expressing GCaMP6s. Yellow arrowhead indicates activated SST-IN soma. Scale bar, 200 μm in middle panel and 50 μm in right panel.

(B) Schematic diagram showing two-photon imaging planes in the superficial layer of the motor cortex.

(C–E) (C) Representative fluorescence traces of GCaMP6s-labeled SST-IN somas before and after MPTP injection. Recording duration: 150 s. (D and E) Distribution (D) and quantitative analysis (E) of total integrated Ca^{2+} in SST-IN somas (t_{129} = 3.15, p = 0.002; n = 65 somas from pre-MPTP and n = 66 somas from post-MPTP in four mice).

(F) Representative Ca^{2+} traces of SST-IN axons before and after MPTP injection.

(G and H) Distribution (G) and quantitative analysis (H) of total integrated Ca^{2+} in SST-IN axons (t_{334} = 6.011, p < 0.0001; n = 182 axons from pre-MPTP and n = 154 axons from post-MPTP in four mice).

*p < 0.05. Data were presented as mean ± SEM.

the activity of SST-IN somas was significantly reduced within 1 h after MPTP injection (p < 0.01 by t test, Figures 4C–4E). This reduction in SST-IN activity was also observed in their axon fibers projecting to layer 1 (p < 0.01 by t test, Figures 4F–4H), indicating that MPTP induces a marked reduction of SST-IN activities in the motor cortex.

Activation of SST-INs Reduces Dendritic Ca^{2+} Spikes in MPTP-Treated Mice

Previous studies have shown that SST-INs regulate dendritic Ca^{2+} spike generation in apical tuft dendrites of pyramidal neurons (Cichon et al., 2017). To test whether the decreased SST-IN activity contributes to MPTP-induced dendritic Ca^{2+} spikes in L5PRNs, we activated SST-INs *in vivo* by using the designer receptors exclusively activated by designer drugs (DREADD). In this experiment, we infected SST-INs in the

motor cortex with AAV encoding Cre-dependent hM3Dq DREADD receptors in SST-*IRES*-Cre mice (Figure 5A). An i.p. injection of DREADD receptor ligand, clozapine-N-oxide (CNO), selectively activated hM3Dq-expressing SST-INs as reported by cFos immunostaining (Figure 5B). To test the effect of SST-IN activation on MPTP-induced dendritic activity in L5PRNs, we imaged GCaMP6s-expressing apical dendrites in mice expressing hM3Dq in SST-INs (Figures 5A and S3). Dendritic Ca^{2+} activities were measured before and after CNO injection in MPTP-treated mice. We found that activation of SST-INs substantially reduced the number of dendritic Ca^{2+} spikes within 1 h and such effects persisted for at least 4 h ($p < 0.0001$ by two-way ANOVA, Figures 5C–5E, Video S3). Analyses of individual dendrites revealed a reduction of both Ca^{2+} spikes' frequency and total integrated Ca^{2+} levels after the activation of SST-INs ($p < 0.001$ by t test, Figures 5F and 5G). Comparing among all the treatment groups, activation of SST-INs reduced the number of dendritic Ca^{2+} spikes in MPTP-treated mice to levels that are comparable with the pre-MPTP group (Figure S4). Taken together, these findings indicate that activation of SST-INs in the motor cortex is sufficient to suppress pyramidal neuron dendritic hyperexcitability induced by MPTP.

Activation of SST-INs Alleviates Dendritic Spine Instability and Motor Memory Deficits

We next investigated whether activation of SST-INs could rescue dendritic spine loss and motor memory deficits induced by acute MPTP infection. We crossed SST-*IRES*-Cre mice with *Thy1*-YFP mice and bilaterally injected Cre-dependent AAV-dio-hM3Dq-mCherry into the primary motor cortex (Figure 6A). Mice were trained on the accelerating rotarod motor learning task and administered MPTP and CNO 8 h after training. The cFos immunofluorescent staining showed that a single injection of CNO activated more than 75% of hM3Dq-expressing cells (Figure 6B). When dendritic spine plasticity was examined, we found that CNO treatment significantly increased the survival rates of learning-induced new spines in the motor cortex ($p < 0.01$ by t test for both 8–12 h and 8–24 h, Figures 6C and 6D). Furthermore, CNO-treated mice showed higher performance improvement in the rotarod task 24 h or 4 days after initial training ($p < 0.01$ by t test, Figure 6E). Notably, the improvement of rotarod performance positively correlated with the survival rate of training-related persistent new spines ($p = 0.0042$; $r = 0.77$, Figure 6F), suggesting that activation of SST-INs can rescue spine instability and motor memory deficits induced by acute MPTP infusion.

DISCUSSION

In this study, we investigated the effects of acute MPTP treatment on synaptic plasticity and motor memory functions. Using two-photon microscopy, we found that a single injection of MPTP in adolescent mice destabilized dendritic spines on apical dendrites of L5PRNs in the motor cortex, which is associated with an increase of pyramidal neuron dendritic activity and a decrease of SST-IN activity. Notably, activation of SST-INs in the motor cortex following MPTP administration rescued pyramidal cell dendritic and synaptic deficits and preserved motor skill learning memory. Together, our results show that SST-IN dysfunction in the motor cortex plays an important role in synaptic and learning deficits induced by acute MPTP administration. As one parkinsonism-inducing agent, chronic MPTP exposure causes dopamine neuron degeneration, leading to learning and behavioral abnormalities (Guo et al., 2015; Halliday et al., 2014). The current study reported that a single dose of MPTP (30 mg/kg) led to impaired retention of motor skills that were acquired before the MPTP exposure, in association with the loss of learning-related new synapse structure, hyperactivity of pyramidal neuron dendrites, and suppression of SST-IN activity. These results indicate that at early stage of PD, motor cortex dysfunction may form one pathological feature and that targeting SST-INs has the potency to retard the progression of motor syndromes.

Structural and functional synaptic plasticity in the primary motor cortex has been shown to be critical for motor skill learning and retention (Cichon and Gan, 2015; Xu et al., 2009; Yang et al., 2009, 2014). Previous studies reported that rotarod learning over 8 h in 1-month-old mice causes a 2%–4% increase in new spine formation in the motor cortex (Li et al., 2017; Yang et al., 2014). Learning-induced new spines persist over days to weeks, and the survival of these new spines strongly correlates with the animals' performance on motor skill tasks. After acute MPTP administration, we observed a marked increase in dendritic spine dynamics and a substantial loss of learning-induced new spines. This rapid loss of dendritic spines after MPTP exposure may contribute to the impairments of motor skill retention in these mice. To capture the functional plasticity of cortical spines, we employed *in vivo* Ca^{2+} imaging and observed a 3-fold increase in Ca^{2+} activity in dendritic spines after MPTP injection. Previous studies in different neurological diseases, such as seizure (Segal et al., 2000), AD (Bai et al., 2017), and neuropathic pain (Cichon et al., 2017), have
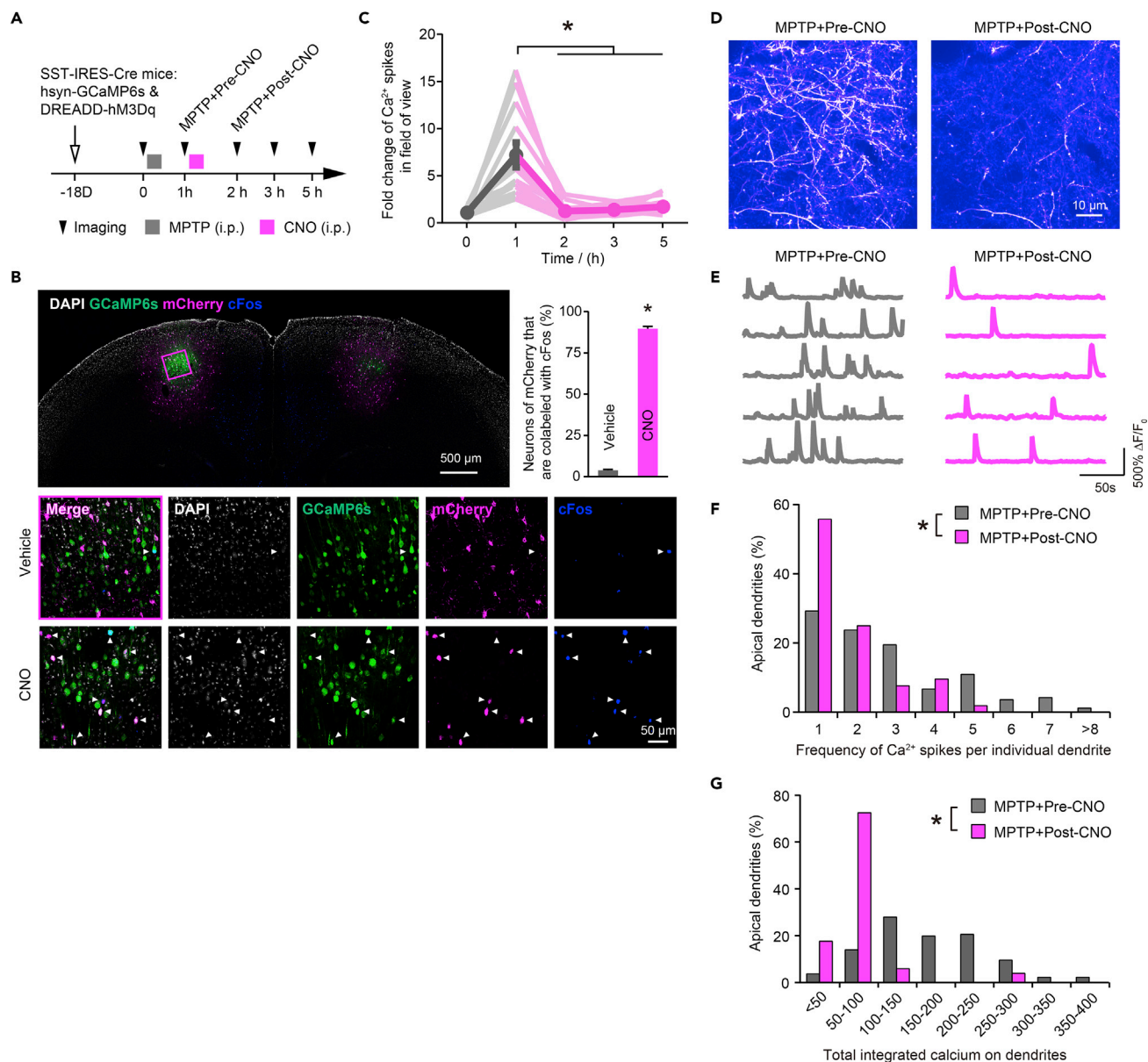
Figure 5. Chemogenetic Activation of SST-INs Reduces MPTP-Induced Pyramidal Neuron Dendritic Activity

(A) Experimental timeline. In brief, AAV-*hsyn*-GCaMP6s and AAV-*dio*-hM3Dq-mCherry viruses were injected into layer 5 and layer 2 or 3 of the motor cortex of SST-*IRES*-Cre mice, respectively. MPTP and CNO were sequentially applied 18 days after viral infection, along with two-photon imaging.

(B) Immunofluorescence images of the motor cortex (upper left and lower panels) showing cFos-positive neurons among mCherry-transfected cells. CNO injection remarkably increased the co-labeling ratio (t_8 = 56.67, p < 0.0001; n = 5 animals per group; upper right panel). Filled arrowheads, cFos-positive neurons. Scale bar, 500 μm in top panel and 50 μm in lower panels.

(C) The frequency of L5PRN dendritic Ca^{2+} spikes in the same field of view (FOV) increased after MPTP administration and decreased after CNO injection ($F_{(3, 48)}$ = 17.98, p < 0.0001; n = 13 FOVs from five mice).

(D and E) (D) Time-series and z-stacked images showing dendritic Ca^{2+} spikes over 50 s in the same FOV before (MPTP + pre-CNO) and after CNO injection (MPTP + post-CNO). Scale bar, 10 μm. (E) Representative fluorescence traces of dendritic Ca^{2+} spikes in L5PRNs.

(F) Distribution of Ca^{2+} spike frequencies in individual dendrites over 3 min before and after MPTP and CNO injection. CNO injection reduced the frequency of dendritic Ca^{2+} spikes (t_{214} = 3.77, p = 0.0002; n = 164 regions of interest from MPTP + pre-CNO and n = 52 from MPTP + post-CNO in four mice).

(G) Ca^{2+} activity in apical dendrites averaged over 3-min recording before and after CNO injection (t_{214} = 5.84, p < 0.0001).

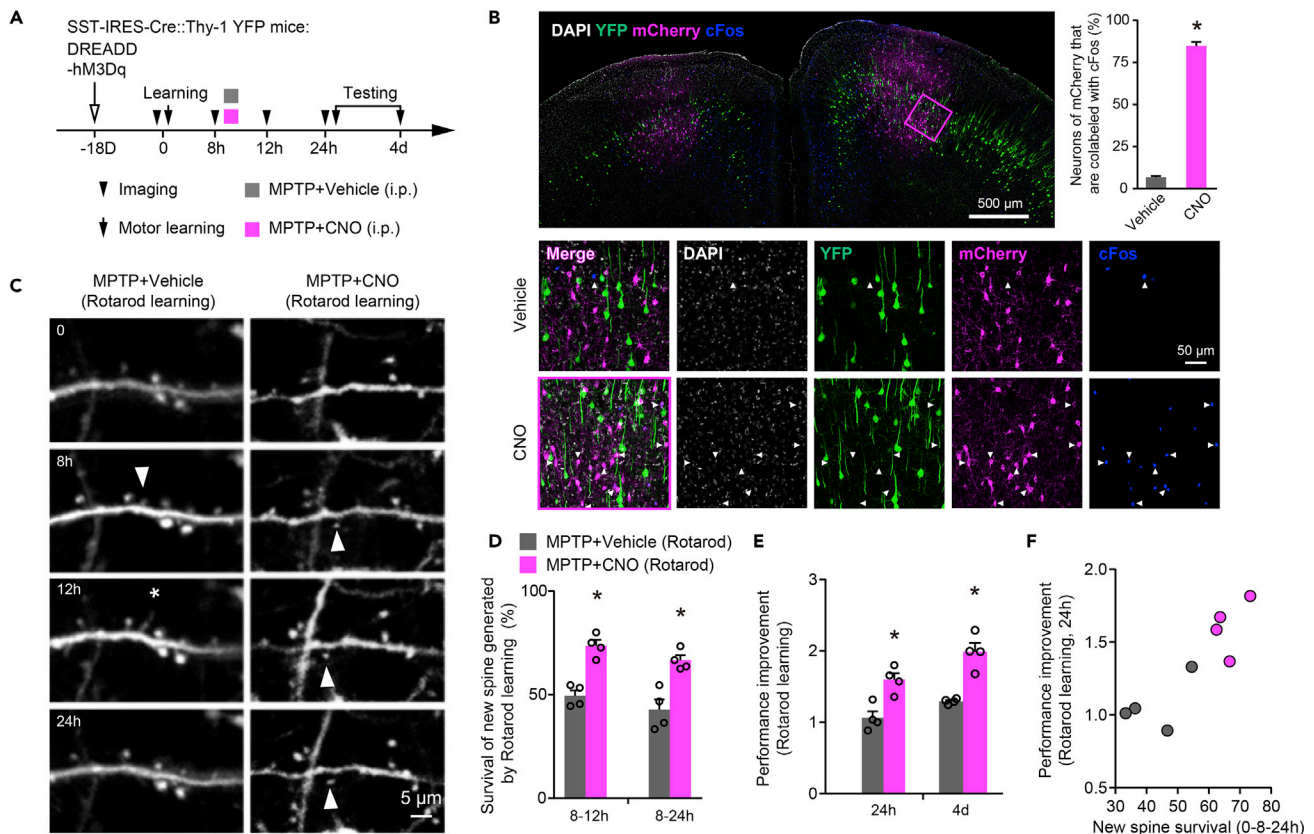*p < 0.05. Data were presented as mean ± SEM. See also Figures S3 and S4.

Figure 6. Activation of SST-INs Alleviates MPTP-Induced Dendritic Spine Loss and Motor Memory Deficits

(A) Experimental timeline.

(B) Immunostaining of the motor cortex (upper left and lower panels) and quantification analysis showing prominent activation of mCherry-positive SST-INs after CNO injection (t_6 = 55.98, p < 0.0001; n = 4 per group). Filled arrowheads, cFos-positive neurons. Scale bar, 500 μm in top panel and 50 μm in lower panels.

(C) Representative dendritic segments from L5PRN apical tufts before rotarod skill learning (0), after learning and MPTP and/or CNO injection (8 h), and afterward (12–24 h). Filled arrowheads, newly formed spines at 8 h; asterisks, filopodia. Scale bar, 5 μm.

(D) CNO injection enhanced the survival rates of newly formed spines within 8- to 12-h and 8- to 24-h time windows (8–12 h, t_6 = 6.35, p = 0.0007; 8–24 h, t_6 = 4.378, p = 0.0047; n = 4 per group).

(E) Performance improvement (fold increase normalized to that in the learning session at 0 h) was elevated at 24 h and 4 days after initial learnings (24 h: t_6 = 4.099, p = 0.0064; 4 days: t_6 = 5.493, p = 0.0015).

(F) Pearson correlation analysis showed positive correlation between new spine survival rates (0–8–24 h) and rotarod performance improvements at 24 h (r = 0.77; p = 0.0042).

*p < 0.05. Data were presented as mean ± SEM.

linked overload of Ca^{2+} to the shrinkage or elimination of dendritic spines. MPTP-induced loss of dendritic spines, therefore, could be attributed to the increased Ca^{2+} transients in pyramidal neuron dendrites and spines. Moreover, we found that MPTP-induced dendritic Ca^{2+} spikes are NMDA receptor dependent, as blockade of NMDA receptor with MK801 normalized dendritic activity in cortical pyramidal neurons. Together, these results suggest that cortical pyramidal neuron dendritic hyperactivity may contribute to MPTP-induced synapse loss and motor memory impairments.

The activities of pyramidal neurons in the cortex are regulated by a great variety of local inhibitory interneurons. Among them, SST-INs constitute ∼30% of all cortical interneurons (Urban-Ciecko and Barth, 2016). Although SST-INs themselves are a heterogeneous population and target different cells in different layers, they mainly innervate the distal portion of apical dendrites (Hattori et al., 2017; Muñoz et al., 2017; Urban-Ciecko and Barth, 2016). It has been shown that SST-INs regulate dendritic spine activity and dendritic Ca^{2+} spike generation (Cichon et al., 2017; Cichon and Gan, 2015). Consistent with the increase of dendritic activity in our acute MPTP administration model, we observed a rapid and substantial decrease of SST-IN

activity within 60 min after MPTP infusion, which is in favor of dendritic hyperactivity. Interestingly, measures from postmortem brain of patients with PD-related dementia showed reduced SST immunoreactivity in the cortex (Allen et al., 1985; Beal et al., 1986; Epelbaum et al., 1983), and decreased expression of SST in pluripotent stem cells derived from patients with *Parkin* mutations (Iwasawa et al., 2019), supporting the involvement of SST-INs in PD pathogenesis.

Given the reduction of SST-IN activity after MPTP administration, we manipulated the activity of SST-INs using chemogenetic approach and showed that SST-IN activation in the motor cortex prevented MPTP-induced increase in dendritic Ca^{2+} spike generation (Figure S4), dendritic spine loss, and motor memory impairments. Activation of GABAergic inhibitory interneurons in cortical circuits has been shown to be beneficial in treating multiple neurological disorders with the characteristic of cortical hyperexcitability, including major depressive disorder (Fee et al., 2017; Lin and Sibille, 2015), neuropathic pain (Cichon et al., 2017), AD (Schmid et al., 2016; Verret et al., 2012), and PD (Lindenbach et al., 2016; Tyagi et al., 2015; Zhang et al., 2017). It is worth to note that besides SST-INs, there are other types of inter-neurons located in the superficial layer of the cerebral cortex (Murphy et al., 2016). These cells are known to target apical tuft dendrites, and their activation can suppress Ca^{2+} spike generation in L5PRNs.

To explore the molecular mechanisms underlying MPTP-induced memory deficits, we examined the amounts of various proteins in the cortex after MPTP treatment, focusing on those involved in synaptic plasticity and function (Lee et al., 2009; Yasuda, 2017). Previous studies have shown that activation of Ca^{2+}/calmodulin-dependent kinase II (CaMKII) (Adler et al.; Lee et al., 2009; Lisman et al., 2012) and small GTPase proteins (Hedrick et al., 2016) facilitates the long-term potentiation of dendritic spines in hippo-campal slices. Using western blot analysis, we found that MPTP injection had no significant effects on the total amounts of CaMKII in the brain but caused a marked reduction in the level of CaMKII phosphory-lated at Thr-286 (p-CaMKII) when compared with vehicle-treated controls at 4–12 h (Figure S5). These results indicate that MPTP treatment acutely impairs CaMKII autophosphorylation in the cortex. Impor-tantly, CNO treatment of SST-*IRES*-Cre mice infected with hM3Dq exhibited normal levels of p-CaMKII 4 h after MPTP injection, whereas the levels of cofilin, Ras1, RhoA, cdc42, and Rac1 remained unaltered (Figure S5). CaMKII autophosphorylation is an important regulator of synaptic plasticity (Chang et al., 2017; Lee et al., 2009; Okamoto et al., 2007), and its impairments have been observed in mouse hippo-campus after acute or chronic MPTP infusion (Zhu et al., 2015). More importantly, a recent study sug-gested that pharmacological inhibition of CaMKII phosphorylation can disrupt motor learning (Adler et al., 2019). The fact that SST-IN activation also corrects CaMKII autophosphorylation further suggests that manipulating SST-IN activity could be an important approach for preventing cortical hyperexcitabil-ity and motor memory impairments.

In sum, our current work demonstrates rapidly hyperactivated dendritic spines in the motor cortex after acute MPTP infusion, in association with spine loss plus motor dysfunctions. The activation of SST-INs helps to relieve these pathological phenotypes to recover motor learning function. Future studies will be needed to examine whether other types of interneurons could also be targeted to protect synaptic loss and motor learning deficits in MPTP-treated mice.

Limitations of the Study

Our results demonstrate that potentiation of cortical SST-INs could relieve dendritic hyperactivity, spine loss, and motor learning deficits after acute MPTP injection. The current study, however, does not address if similar strategy can be used under chronic MPTP administration, which is one typical model of PD. More-over, the long-term ameliorating effect from chemogenetics activation approach has not been evaluated. Further studies are thus required to address those issues to get a more complete picture of inhibitory transmission in motor cortical dysfunction.

METHODS

All methods can be found in the accompanying Transparent Methods supplemental file.

SUPPLEMENTAL INFORMATION

Supplemental Information can be found online at https://doi.org/10.1016/j.isci.2019.06.040.

REFERENCES

Adler, A., Zhao, R., Shin, M.E., Yasuda, R., and Gan, W.-B. (2019). Somatostatin-expressing interneurons enable and maintain learning-dependent sequential activation of pyramidal neurons. Neuron 102, 202–216.e7.

Allen, J.M., Cross, A.J., Crow, T.J., Javoy-Agid, F., Agid, Y., and Bloom, S.R. (1985). Dissociation of neuropeptide Y and somatostatin in Parkinson's disease. Brain Res. 337, 197–200.

Bai, Y., Li, M., Zhou, Y., Ma, L., Qiao, Q., Hu, W., Li, W., Wills, Z.P., and Gan, W.-B. (2017). Abnormal dendritic calcium activity and synaptic depotentiation occur early in a mouse model of Alzheimer's disease. Mol. Neurodegener. 12, 86.

Beal, M.F., Mazurek, M.F., and Martin, J.B. (1986). Somatostatin immunoreactivity is reduced in Parkinson's disease dementia with Alzheimer's changes. Brain Res. 397, 386–388.

Chang, J.-Y., Parra-Bueno, P., Laviv, T., Szatmari, E.M., Lee, S.-J.R., and Yasuda, R. (2017). CaMKII autophosphorylation is necessary for optimal integration of Ca2+ signals during LTP induction, but not maintenance. Neuron 94, 800–808.e4.

Chen, C.C., Lu, J., Yang, R., Ding, J.B., and Zuo, Y. (2018). Selective activation of parvalbumin interneurons prevents stress-induced synapse loss and perceptual defects. Mol. Psychiatry 23, 1614–1625.

Cichon, J., Blanck, T.J.J., Gan, W.B., and Yang, G. (2017). Activation of cortical somatostatin interneurons prevents the development of neuropathic pain. Nat. Neurosci. 20, 1122–1132.

Cichon, J., and Gan, W.B. (2015). Branch-specific dendritic Ca(2+) spikes cause persistent synaptic plasticity. Nature 520, 180–185.

Epelbaum, J., Ruberg, M., Moyse, E., Javoy-Agid, F., Dubois, B., and Agid, Y. (1983). Somatostatin and dementia in Parkinson's disease. Brain Res. 278, 376–379.

Fee, C., Banasr, M., and Sibille, E. (2017). Somatostatin-positive gamma-aminobutyric acid interneuron deficits in depression: cortical microcircuit and therapeutic perspectives. Biol. Psychiatry 82, 549–559.

Guo, L., Xiong, H., Kim, J.-I., Wu, Y.-W., Lalchandani, R.R., Cui, Y., Shu, Y., Xu, T., and Ding, J.B. (2015). Dynamic rewiring of neural circuits in the motor cortex in mouse models of Parkinson's disease. Nat. Neurosci. 18, 1299.

Halliday, G.M., Leverenz, J.B., Schneider, J.S., and Adler, C.H. (2014). The neurobiological basis of cognitive impairment in Parkinson's disease. Mov. Disord. 29, 634–650.

Hattori, R., Kuchibhotla, K.V., Froemke, R.C., and Komiyama, T. (2017). Functions and dysfunctions of neocortical inhibitory neuron subtypes. Nat. Neurosci. 20, 1199–1208.

Hedrick, N.G., Harward, S.C., Hall, C.E., Murakoshi, H., McNamara, J.O., and Yasuda, R. (2016). Rho GTPase complementation underlies BDNF-dependent homo- and heterosynaptic plasticity. Nature 538, 104.

Iwasawa, C., Kuzumaki, N., Suda, Y., Kagawa, R., Oka, Y., Hattori, N., Okano, H., and Narita, M. (2019). Reduced expression of somatostatin in GABAergic interneurons derived from induced pluripotent stem cells of patients with parkin mutations. Mol. Brain 12, 5.

Lee, S.-J.R., Escobedo-Lozoya, Y., Szatmari, E.M., and Yasuda, R. (2009). Activation of CaMKII in single dendritic spines during long-term potentiation. Nature 458, 299–304.

Li, W., Ma, L., Yang, G., and Gan, W.-B. (2017). REM sleep selectively prunes and maintains new synapses in development and learning. Nat. Neurosci. 20, 427–437.

Lin, L.C., and Sibille, E. (2015). Somatostatin, neuronal vulnerability and behavioral emotionality. Mol. Psychiatry 20, 377–387.

Lindenbach, D., Conti, M.M., Ostock, C.Y., George, J.A., Goldenberg, A.A., Melikhov-Sosin, M., Nuss, E.E., and Bishop, C. (2016). The role of primary motor cortex (M1) glutamate and GABA signaling in DOPA-Induced Dyskinesia in Parkinsonian rats. J. Neurosci. 36, 9873–9887.

Lisman, J., Yasuda, R., and Raghavachari, S. (2012). Mechanisms of CaMKII action in long-term potentiation. Nat. Rev. Neurosci. 13, 169–182.

Muñoz, W., Tremblay, R., Levenstein, D., and Rudy, B. (2017). Layer-specific modulation of neocortical dendritic inhibition during active wakefulness. Science 355, 954–959.

Murphy, S.C., Palmer, L.M., Nyffeler, T., Müri, R.M., and Larkum, M.E. (2016). Transcranial magnetic stimulation (TMS) inhibits cortical dendrites. Elife 5, e13598.

Okamoto, K.-I., Narayanan, R., Lee, S.H., Murata, K., and Hayashi, Y. (2007). The role of CaMKII as an F-actin-bundling protein crucial for maintenance of dendritic spine structure. Proc. Natl. Acad. Sci. U S A 104, 6418–6423.

Pelled, G., Bergman, H., and Goelman, G. (2002). Bilateral overactivation of the sensorimotor cortex in the unilateral rodent model of Parkinson's disease – a functional magnetic resonance imaging study. Eur. J. Neurosci. 15, 389–394.

Sabatini, U., Boulanouar, K., Fabre, N., Martin, F., Carel, C., Colonnese, C., Bozzao, L., Berry, I., Montastruc, J.L., Chollet, F., et al. (2000). Cortical motor reorganization in akinetic patients with Parkinson's disease A functional MRI study. Brain 123, 394–403.

Schmid, L.C., Mittag, M., Poll, S., Steffen, J., Wagner, J., Geis, H.R., Schwarz, I., Schmidt, B., Schwarz, M.K., Remy, S., et al. (2016). Dysfunction of somatostatin-positive interneurons associated with memory deficits in an Alzheimer's disease model. Neuron 92, 114–125.

Segal, M., Korkotian, E., and Murphy, D.D. (2000). Dendritic spine formation and pruning: common cellular mechanisms? Trends Neurosci. 23, 53–57.

Tyagi, R.K., Bisht, R., Pant, J., Kumar, P., Majeed, A.B.A., and Prakash, A. (2015). Possible role of GABA-B receptor modulation in MPTP induced Parkinson's disease in rats. Exp. Toxicol. Pathol. 67, 211–217.

Urban-Ciecko, J., and Barth, A.L. (2016). Somatostatin-expressing neurons in cortical networks. Nat. Rev. Neurosci. 17, 401.

Verret, L., Mann, E.O., Hang, G.B., Barth, A.M., Cobos, I., Ho, K., Devidze, N., Masliah, E., Kreitzer, A.C., Mody, I., et al. (2012). Inhibitory interneuron deficit links altered network activity and cognitive dysfunction in Alzheimer model. Cell 149, 708–721.

Weber, J.P., Andrasfalvy, B.K., Polito, M., Mago, A., Ujfalussy, B.B., and Makara, J.K. (2016). Location-dependent synaptic plasticity rules by dendritic spine cooperativity. Nat. Commun. 7, 11380.

Xu, N.L., Harnett, M.T., Williams, S.R., Huber, D., O'Connor, D.H., Svoboda, K., and Magee, J.C. (2012). Nonlinear dendritic integration of sensory and motor input during an active sensing task. Nature 492, 247–251.

Xu, T., Yu, X., Perlik, A.J., Tobin, W.F., Zweig, J.A., Tennant, K., Jones, T., and Zuo, Y. (2009). Rapid formation and selective stabilization of synapses for enduring motor memories. Nature 462, 915–919.

Yang, G., Lai, C.S.W., Cichon, J., Ma, L., Li, W., and Gan, W.-B. (2014). Sleep promotes branch-specific formation of dendritic spines after learning. Science 344, 1173–1712.

Yang, G., Pan, F., and Gan, W.B. (2009). Stably maintained dendritic spines are associated with lifelong memories. Nature 462, 920–924.

Yasuda, R. (2017). Biophysics of biochemical signaling in dendritic spines: implications in synaptic plasticity. Biophys. J. 113, 2152–2159.

Yu, H., Sternad, D., Corcos, D.M., and Vaillancourt, D.E. (2007). Role of hyperactive cerebellum and motor cortex in Parkinson's disease. NeuroImage 35, 222–233.

Zhang, T., Chen, T., Chen, P., Zhang, B., Hong, J., and Chen, L. (2017). MPTP-induced dopamine depletion in Basolateral Amygdala via decrease of D2R activation suppresses GABAA receptors expression and LTD induction leading to anxiety-like behaviors. Front. Mol. Neurosci. 10, 247.

Zhu, G., Li, J., He, L., Wang, X., and Hong, X. (2015). MPTP-induced changes in hippocampal synaptic plasticity and memory are prevented by memantine through the BDNF-TrkB pathway. Br. J. Pharmacol. 172, 2354–2368.

Supplemental Information

Activation of Cortical Somatostatin Interneurons

Rescues Synapse Loss and Motor Deficits

after Acute MPTP Infusion

Kai Chen, Guang Yang, Kwok-Fai So, and Li Zhang
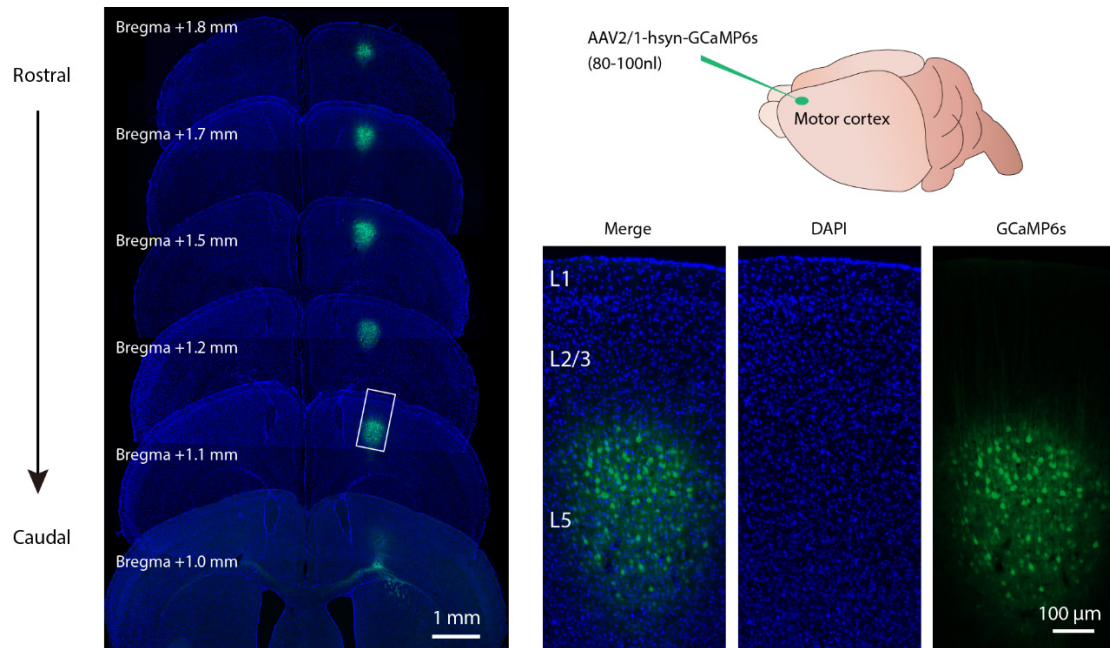
Supplemental Information

Fig. S1. Verification of AAV-GCaMP6s injection sites, **related to Fig. 2.** Left panels, series of coronal sections showing injection sites within the primary motor cortex. Right panels, enlarged views (white rectangle on the left) showed that most of GCaMP6s transfected neurons were located within layer 5 but not in the layer 2/3.
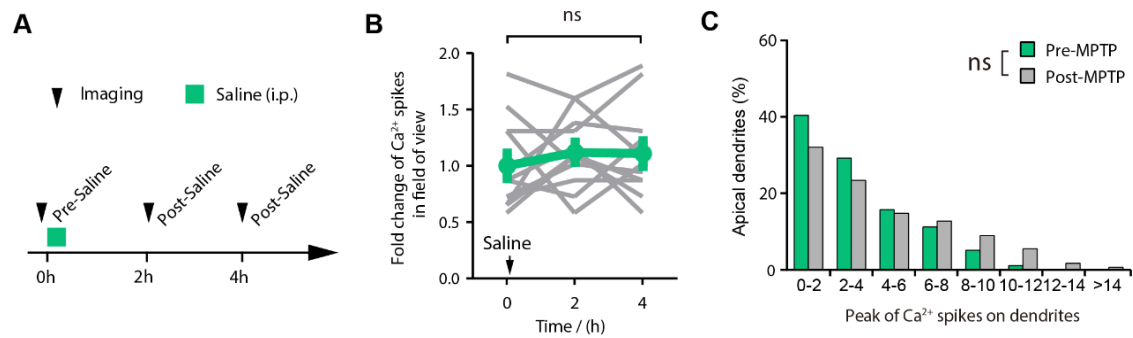
Fig. S2. Analyses of dendritic Ca²⁺ spikes after saline or MPTP injection, **related to Fig. 2.** (**A**) Experimental timeline. (**B**) Dendritic Ca²⁺ spike frequency before and after saline injection ($F_{(2, 33)}$ = 0.38, P = 0.68; n = 3). (**C**) Distribution of dendritic Ca²⁺ spike amplitudes before and after MPTP injection. MPTP has no effect on the peak amplitude of dendritic Ca²⁺ spikes (t_{305} = 0.857, P = 0.6225; n = 5). ns, non-significant difference. Data were presented as mean ± s.e.m.
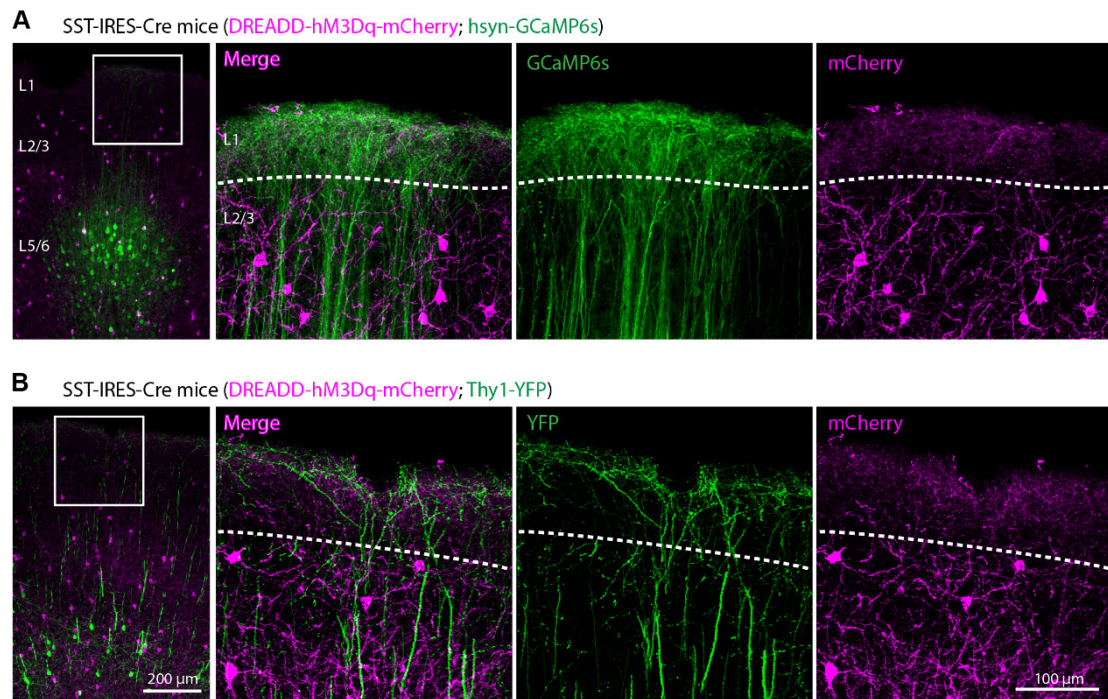
Fig. S3. AAV-infected cells in the primary motor cortex, related to Fig. 5. (**A**) Representative fluorescence images showing the primary motor cortex of an SST-*IRES*-Cre mouse with AAV-hSyn-GCaMP6s injected into layer 5 and AAV-hM3Dq-mCherry injected into layer 2/3. Apical tufts of L5 pyramidal neurons (L5PRNs) expressing GCaMP6s are seen in layer 1, while somas of mCherry-labeled SST+ interneurons (SST-INs) are within layer 2/3. (**B**) Representative fluorescence images showing the motor cortex of an SST-*IRES*-Cre::*Thy1*-YFP mouse that were injected with AAV-hM3Dq-mCherry virus. YFP-labeled L5PRNs project their apical tuft dendrites to layer 1, while axons of mCherry-labeled SST-INs are morphologically distinct from pyramidal neuron dendrites.
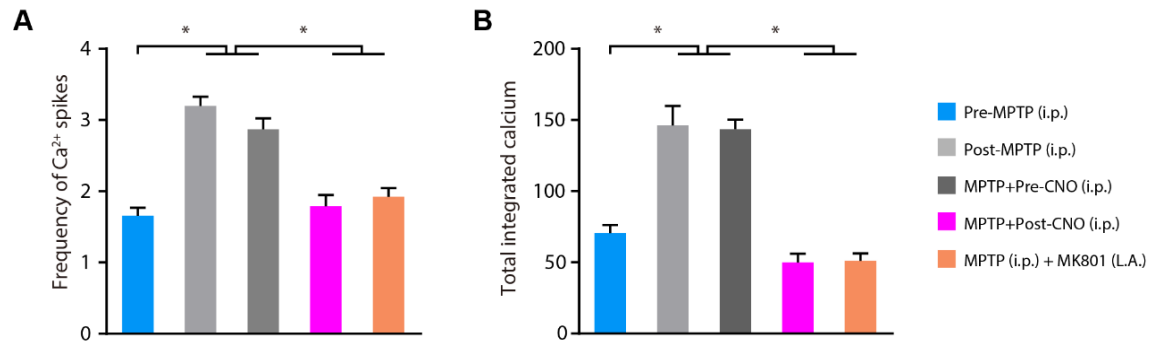
Fig. S4. MPTP-induced dendritic hyperactivity are reversed by activation of SST+ interneurons or MK801 local infusion, related to Fig. 5. (A) Frequency of dendritic Ca^{2+} spikes before and after MPTP and CNO or MK801 administration ($F_{(4, 606)}$ = 18.27, $P < 0.0001$) (B) Dendritic Ca^{2+} activity before and after MPTP and CNO or MK801 administration ($F_{(4, 606)}$ = 31.11, $P < 0.0001$). *$P < 0.05$. Data were presented as mean ± s.e.m. i.p., intraperitoneal injection; L.A., local application.
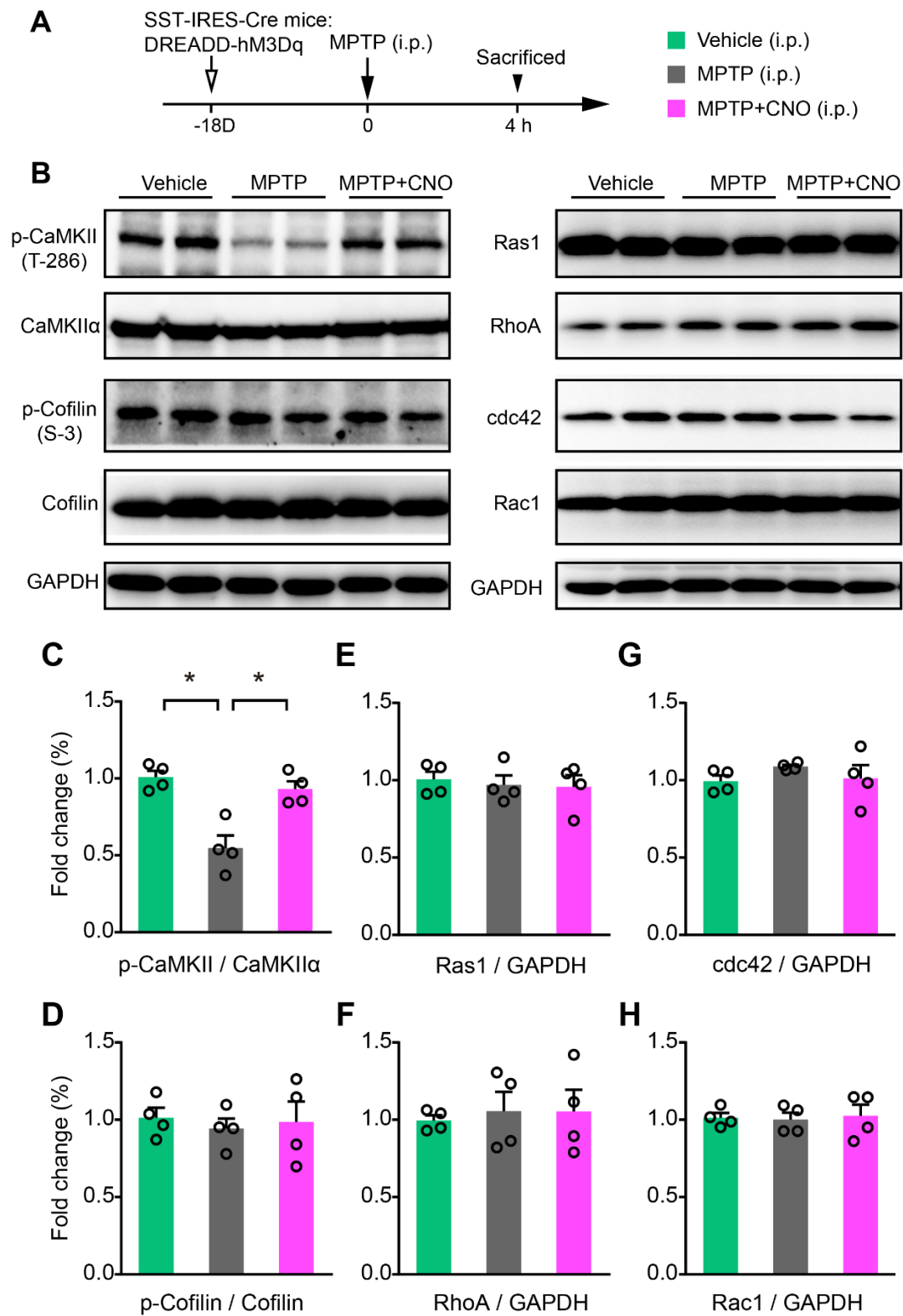
Fig. S5. Activation of SST-INs prevents MPTP-induced reduction of CaMKII autophosphorylation. (**A**) Experimental timeline. Protein samples were collected from the motor cortex at 0, 4, 12 and 24 h after MPTP injection. (**B**) Western blotting bands showing phosphorylated CaMKII (p-CaMKII), total CaMKIIα, p-Cofilin, total

Cofilin, Ras1, RhoA, Cdc42 and Rac1. (**C to H**) Quantification of relative protein expression levels. Among all proteins examined, only p-CaMKII level was decreased 4 and 12 h after MPTP injection but recovered 24 h later. (All test statistics: p-CaMKII, $F_{(3, 8)} = 8.763$, $P = 0.0066$; CaMKII, $F_{(3, 8)} = 0.8068$, $P = 0.5246$; Phosphorylated cofilin/ total cofilin, $F_{(2, 9)} = 0.1470$, $P = 0.8653$; Ras1, $F_{(2, 9)} = 0.1568$, $P = 0.8571$; RhoA ($F(2, 9) = 0.0969$, $P = 0.9085$; Cdc42, $F_{(2, 9)} = 0.8152$, $P = 0.4727$; Rac1, $F_{(2, 9)} = 0.05478$, $P = 0.9470$); $n = 4$ for each group. * $P < 0.05$. Data are presented as mean ± s.e.m.

Transparent Methods

Experimental animals

Thy1-yellow fluorescent protein (YFP) transgenic mice and SST-*IRES*-Cre mice were purchased from Jackson Laboratory, bred in-house, and were used for dendritic spine imaging and chemogenetic assays. Male C57BL/6J mice were purchased from Guangdong Medical Laboratory Animal Center and were used for all experiments. For spine structural imaging (Fig. 1), 30-day old male *Thy1*-YFP mice were used. For *in vivo* Ca^{2+} imaging (Fig.2 to Fig. 4), male C57 mice (Fig.2 and Fig. 3) or SST-Cre mice (Fig. 4) received virus injection at P30, and were imaged 18 days later. In chemogenetic study (Fig. 5 and Fig. 6), SST-Cre::*Thy1*-YFP mice (Fig. 5) or SST-Cre mice (Fig. 6) received combined virus injection at P30, and were imaged after 18 days. All experimental animals were group-housed in the normal light-dark cycle (08:00-20:00 on light) with food and water *ad libitum*. In chemogenetics assays, CNO (2.5mg/kg) was applied by intraperitoneal injection. All experimental protocols have been pre-approved by the laboratory Animal Ethics Committee at Jinan University in accordance with IACUC guidelines for animal research.

Motor learning assays

All behavioral experiments were performed in a blinded manner. The rotarod task was performed using the Rotamex Rotarod apparatus (UGO Basile Mouse Rota-Rod 47700/600, Italy). During the learning phase, the mice were trained under an accelerating mode (2 to 80 rpm over the course 5 min) for multiple sessions until more than 50% improvements of latencies have been observed compared to those during the initial training session. The single retrieval test was performed at 24 h and 4 days later using the same parameter as the training sessions. The performance improvement is calculated as (Latency of test session – latency of training session) / Latency of training session.

In the beam walking test, a customized walking beam (70cm length, 6cm width) was connected with two-side chambers. The whole apparatus was placed 60 cm above the floor. The mouse was trained to walk cross the beam to reach the other chamber

and the time duration on the beam was recorded. In general, the mice were trained for 3 or more consecutive sessions with 5 min interval to reach a stable performance without interruption during the beam-walking session. The memory retrieval session was performed 24 h later. The performance improvement was calculated as (Averaged crossing time in training sessions – crossing time in testing session) / Averaged crossing time in training sessions.

Stereotaxic injection of viral vectors

Genetically encoded calcium indicator GCaMP6s was packaged into adeno-associated virus (AAV, serotype 2/1, viral titer>2×10^{13} genome copies per ml) under human synapsin (hSyn) promotor (Gene Therapy Program Vector Core, University of Pennsylvania). For stereotaxic injection, mice were anesthetized by intraperitoneal injection of 1.25% Avertin. The primary motor cortex (0.5 mm anterior to the Bregma and 1.2 mm lateral) was identified by a stereotaxic instrument (RWD, China). A high-speed microdrill was used to create an injection hole, through which 80–100 nl of AAV-hSyn-GCaMP6s vector was injected into the motor cortex at 25 nl per min velocity using glass micropipette connected to an ultra-micro injection pump (Nanoliter2010, WPI, USA) under a controller (Micro4, WPI, USA). The micropipette was retained in layer 5 (500-700 μm depth from the pia) for 10 min before retraction. A 60° injection angle was adopted to avoid damaging the neurons and dendrites of the imaging area. The Ca^{2+} imaging assay was performed 18 days after virus injection. To monitor SST-IN activity, AAV-CAG-Flex-GCaMP6s (Serotype 2/1, viral titer > 2×10^{13} genome copies per ml, Penn Vector Core) was injected into the primary motor cortex of SST-*IRES*-Cre mice. For chemogenetic manipulation assays, 200–300 nl of AAV-hSyn-DIO-hM3Dq-mCherry vector (Serotype 2/9, 2×10^{12} genome copies per ml, Taitool BioScience Co, Shanghai) was bilaterally injected into the primary motor cortex of SST-*IRES*-Cre mice, and 80–100 nl of AAV-*hSyn*-GCaMP6s vector was separately injected into layer 5. For chemogentic coupled with spine imaging assays, 200 nl of AAV-*hSyn*-DIO-hM3Dq-mCherry vector were bilaterally injected into layer 2/3 of the

primary motor cortex of *Thy1*-YFP::SST-*IRES*-Cre mice. The expression of the virus in the primary motor cortex was further validated by fixation, sectioning and fluorescence imaging after 2-photon microscopy.

In vivo two-photon imaging of spine structure and Ca^{2+} spikes

The structural plasticity of dendritic spines was observed using the thin-skull approach. In brief, mice were anesthetized with 1.25% Avertin. Their eyes were protected by the eye ointment, the head hair was shaved, and the skull surface was exposed and cleaned. The primary motor cortex was identified by a stereotactic apparatus and marked. A double-sided blade was glued to the targeted imaging region and a customized stage was used to fix the skull. A circular imaging window was created by high-speed microdrill and microsurgical blade. The skull was covered with artificial cerebrospinal fluid (ACSF), and the mouse was placed on the stage of two-photon microscope (LSM780, Zeiss, Germany). Images of apical dendritic spines were captured under a water-immersed 20× objective (1.1NA) using 920 nm excitation wavelength for YFP. A low-magnification z-stacked image (1× digital zoom, 512 × 512 pixels) and the blood vessel map were recorded for the future re-imaging. About seven high-magnification z-stacked images (4× digital zoom, 0.75 μm step size, 1024 × 1024 pixels) were acquired for dendritic spine quantification. One imaging session took ~30 min. After imaging, the mouse head was gently detached from the skull holder. The remaining glue was cleaned, and the scalp was sutured by surgical silk. Mice were returned to their own home cages for post-op recovery until the next imaging session.

For *in vivo* Ca^{2+} imaging, the surgical procedures were performed 24 h in advance and a custom-made head holder was glued and attached to the skull. The dental acrylic cement was used to seal the reaming part of the skull except for the imaging region. After surgical recovery, the mouse was returned to their home cage for imaging.

To capture Ca^{2+} activity of L5 PRN dendrites and SST-IN axons or somas, an imaging window was created by removing a small piece (2 mm × 2 mm) of skull

above the motor cortex using a high-speed microdrill. The window was covered with a glass coverslip before imaging. Ca^{2+} activities of both dendrites and somas were recorded at 2 Hz with a water-immersed 20× objective (1.1NA, 2× digital zoom) for 3 min and 2.5 min, respectively. During imaging, the laser power at 920 nm was less than 25 mW to prevent possible tissue injury or bleaching effects.

Local application of drugs

After imaging session, a small bone flap adjacent to the imaging window was removed by a high-speed microdrill. 200 nl of NMDAR antagonist MK801 (HY-15084, 10μM in ACSF, MedChemExpress, US) was applied onto the superficial layer with an angle of 60° using a micropipette. In general, the injection site was >100 μm away from imaging region to avoid tissue injury.

In the local administration assay, 100 μl MPTP (30 μM in the ACSF, HY-15608, MedChemExpress, US) was immersed onto the brain surface through the hole created by the high-speed microdrill with ~1 mm adjacent to the imaging window. The drug immersion lasted for ~30 min, followed by the re-imaging session.

Western blotting

Total protein samples were extracted from the motor cortex as abovementioned. The protein concentration was determined by a BCA kit (Beyotime, China). 10 μg/ml protein samples were mixed with 5X bromophenol blue at 4:1 ratio and boiled at $100^{o}C$ for 10 min before loading. 10% polyacrylamide gel (10% SDS, 1.5M Tris-Hcl, 40% acrylamide, APS and TEMED) was used for SDS-PAGE assays. In each well, 8 μl protein was loaded for 120 min electrophoresis, and protein samples were then transferred to the polyvinylidene fluoride membrane (PVDF) within 80 min. The membranes were washed by the PBST and were blocked with 5 % bovine serum album (BSA) at RT for 2 h. The primary antibody was then used for $4^{o}C$ overnight incubation, including p-CaMKII (#3356, Cell Signal Technology, US), CaMKIIα (#50049, Cell Signal Technology), p-Cofilin (#3311, Cell Signal Technology), Cofilin (#5175, Cell Signal Technology), Rac1 (#2465, Cell Signal Technology), Ras1 (#3965,

Cell Signal Technology), RhoA (#8084, Cell Signal Technology), Cdc42 (#2462, Cell Signal Technology), GAPDH (#ab9484, Abcam) and Actin (#8457, Cell Signal Technology). After primary antibody, the membrane was washed for 6 times and then incubated with secondary antibody (anti-rabbit IgG and anti-mouse IgG) for 2 h at RT. After washing out the excessive secondary antibody, the protein band was visualized by a protein imaging system (Bio-Rad, US), and was identified under the help of 11-250 kDa ladder (Abcam). The band density was analyzed by ImageJ.

Immunofluorescent staining

Deeply anesthetized mouse was perfused with saline and 4% paraformaldehyde (PFA). The mouse brain was fixed in PFA overnight and dehydrated by 30% sucrose for 24–48 h. The whole brain was sectioned into 40 μm coronal slices by a microtome (SM2010R, Leica, Germany). Brain slices were washed in PBS containing 0.25% Triton X-100 and were blocked for 2 h at RT. Those slices were incubated at $4^{\circ}C$ overnight in primary antibody anti-cFos (#2250, Cell Signal Technology). Secondary antibodies (Alexa Fluor 594/647 conjugated donkey anti-rabbit) were added after washing out the primary antibody. Tissue sections were mounted onto SuperFrost slides (Fisher scientific, US). Image stacks were captured with a confocal microscope (LM710, Zeiss) using 10× and 20× objectives. The ImageJ software was used for cell counting and density analysis.

Statistical analysis

All results are reported as mean ± s.e.m. Statistical analyses were performed using Prism v7.0 (GraphPad, US). Imaging data were analyzed with ImageJ or Fiji (NIH, US). Student t-test was used for comparison of means between two groups. For multi-group comparison, one-way or two-way analysis of variance (ANOVA) was employed, followed by Tukey's *post-hoc* comparisons. A statistical significance was defined at $P < 0.05$.

Data and software availability

All data are included in the manuscript and/or in the Supplementary Information. Additional data related to this study may be available from the lead contact (L.Z.) upon request.